Volume 3
Number 4
April 2024
Pages 667–918

Energy Advances

rsc.li/energy-advances

ISSN 2753-1457

ROYAL SOCIETY OF CHEMISTRY

PAPER
Yutaka Moritomo *et al.*
Precipitation enhancement of liquid thermoelectric conversion with $Fe(ClO_4)_2/Fe(ClO_4)_3$ dissolved in DMF

Energy Advances

ROYAL SOCIETY OF CHEMISTRY

PAPER

View Article Online
View Journal | View Issue

Cite this: *Energy Adv.*, 2024, 3, 784

Precipitation enhancement of liquid thermoelectric conversion with $Fe(ClO_4)_2/Fe(ClO_4)_3$ dissolved in DMF

Akihiro Wake,[a] Dai Inoue[a] and Yutaka Moritomo *[abc]

Received 24th October 2023,
Accepted 3rd March 2024

DOI: 10.1039/d3ya00516j

rsc.li/energy-advances

The electrochemical Seebeck coefficient α is one of the parameters that determines the performance of liquid thermoelectric conversion devices (LTEs). We systematically investigated α in *N*,*N*-dimethylformamide (DMF) containing both *m* M $Fe(ClO_4)_2$ and *m* M $Fe(ClO_4)_3$ against *m*. Above 0.35 M, we observed significant enhancement of α due to precipitates containing Fe^{3+}. In addition, the precipitation enhances the maximum power of the LTE at 0.4 M by as much as 32%. The precipitation enhancement of α cannot be explained only by the concentration gradient model. We propose a solution-solid equilibrium of Fe^{3+} as an additional precipitate effect, which can fill the difference between the concentration gradient model and observed α.

1 Introduction

In recent years, research and development of energy harvesting technologies[1–3] have been vigorously carried out to achieve the sustainable development goals (SDGs) and prevent global warming by reducing CO_2. Among the energy harvesting technologies, liquid thermoelectric conversion devices (LTEs), which have a simple device structure composed of low-cost materials, are attracting attention. Although the history of LTE research and development is very long,[4–22] vigorous research and development continues even now.[23–32] The thermoelectromotive force V_T of an LTE is expressed as $V_T = \alpha(T_H - T_L)$, where T_H and T_L are the temperatures at the high and low temperature electrodes, respectively. From a technical point of view, 20 mV is the minimum value to drive a semiconductor device, because a commercially available booster circuit can boost 20 mV to several volts. An LTE can achieve this value with a ΔT (= $T_H - T_L$) of about 20 K. The performance of LTEs is governed by the electrochemical Seebeck coefficient α, electric conductivity σ, and thermal conductivity κ, of the electrolyte. In particular, the dimensionless figure of merit ($ZT = \frac{\alpha^2\sigma T}{\kappa}$, where T is temperature) determines the thermal efficiency of the LTE. To increase ZT, it is necessary to increase α and σ and decrease κ. Until now, aqueous electrolytes were actively investigated as an electrolyte for LTEs. Recently, Inoue *et al.*[33] investigated α in organic electrolytes containing Fe^{2+}/Fe^{3+} and reported that α in several organic electrolytes, *e.g.*, acetone and acetonitrile (AN), surpasses the value (= 1.4 mV K^{-1}) of aqueous electrolytes. In addition, κ ($\approx$ 0.2 W Km^{-1}) of organic solvents is approximately one-third that of water (= 0.6 W Km^{-1}). Therefore, organic electrolytes are promising candidates of electrolytes for high-performance LTEs.[25,26]

Interestingly, addition of other molecules[27–30] or solvents[31] to the electrolyte has been reported to significantly increase α. Zhou *et al.*[27] reported that the addition of cyclodextrins (CD) increases α in the I_3^-/I^- system. They interpreted the enhancement of α in terms of the I_3^- -inclusion by CD and quantitatively explained the observed α based on the Nernst equation including temperature dependence of the association constant. On the other hand, Duan *et al.*[29] reported enhancement of α in aqueous $[Fe(CN)_6]^{4-}/[Fe(CN)_6]^{3-}$ by introducing strong chaotropic cations (guanidinium) and highly soluble amide derivatives (urea). They interpreted the enhancement of α in terms of the enlarged entropy difference in the redox couple. Yu *et al.*[30] reconsidered this enhancement, and interpreted it in terms of the concentration gradient model originated in the temperature dependence of solubility $s(T)$. They presented a qualitative explanation based on the Nernst equation,

$$V = V_0 + \frac{k_B T}{z} \ln \frac{C_{ox}}{C_{re}}, \quad (1)$$

where V, V_0, k_B, z, C_{ox}, and C_{re} are the redox potential, standard redox potential, Boltzmann constant, number of transferred electrons, oxidant concentration, and reductant concentration, respectively. They, however, did not perform quantitative

[a] *Graduate School of Pure & Applied Science, University of Tsukuba, Tennodai 1-1-1, Tsukuba, Ibaraki 305-8571, Japan. E-mail: moritomo.yutaka.gf@u.tsukba.ac.jp*
[b] *Faculty of Pure & Applied Science, University of Tsukuba, Tennodai 1-1-1, Tsukuba, Ibaraki 305-8571, Japan*
[c] *Tsukuba Research Center for Energy Materials Science (TREMS), University of Tsukuba, Tsukuba, Ibaraki 305-8571, Japan*

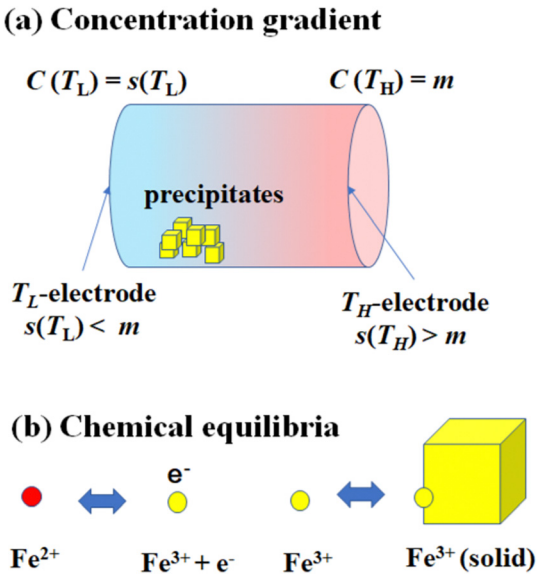

Fig. 1 (a) Schematic illustration of the concentration gradient between the low (T_L) and high (T_H) temperature electrodes. m, $C(T)$, and $s(T)$ are the solute concentration, local concentration, and solubility, respectively. (b) Chemical equilibria in the Fe^{2+}/Fe^{3+} system with precipitates. There exists an equilibrium between Fe^{3+} in solution and Fe^{3+} in solid in addition to that between Fe^{2+} and Fe^{3+} in solutions.

analysis based on $s(T)$. Here, we will quantitatively investigate the precipitation effects on α in a simple solute–solvent system without additional molecules nor solvent.

Fig. 1(a) schematically shows the concentration gradient[30] in between the T_L- and T_H-electrodes. When $s(T_L)$ is below the solute concentration m, precipitation occurs until the local concentration $C(T_L)$ reaches the solubility $s(T_L)$. Then, $C(T_L)$ [= $s(T_L)$.] becomes smaller than $C(T_H)$ (= m). The resultant concentration gradient significantly influences $\alpha \equiv \frac{dV}{dT}$ *via* the second term of the Nernst equation (eqn (1)). Another possible effect of precipitation is additional chemical equilibrium between the solution and solid (precipitate) phases in addition to that between Fe^{2+} and Fe^{3+}, as schematically shown in Fig. 1(b).

In this paper, we systematically investigated α in *N*,*N*-dimethylformamide (DMF) containing both m M $Fe(ClO_4)_2$ and m M $Fe(ClO_4)_3$. Above m = 0.35 M, we observed significant enhancement of α due to precipitates containing Fe^{3+}. The precipitation enhancement of α cannot be explained only by the concentration gradient model. We propose solution-solid equilibrium of Fe^{3+} as another precipitate effect. In addition, the precipitation enhances the maximum power of the LTE at 0.4 M by as much as 32%.

2 Experimental methods

2.1 Preparation and properties of the electrolytes

The electrolytes investigated were DMF solution containing both m M $Fe(ClO_4)_2{\cdot}6H_2O$ and m M $Fe(ClO_4)_3{\cdot}7.1H_2O$. The electrolytes contain the redox pair, that is, Fe^{2+} in a reduced state and Fe^{3+} in an oxidized state, in equal moles. DMF, $Fe(ClO_4)_2{\cdot}6H_2O$, and $Fe(ClO_4)_3{\cdot}7.1H_2O$ were purchased from FUJIFILM Wako corp. and used as received. Fig. 2(a) shows photographs of the DMF solutions at 25 °C. In the DMF solution containing 0.4 M $Fe(ClO_4)_2$ and 0.4 M $Fe(ClO_4)_3$ (upper left) and that containing 0.6 M $Fe(ClO_4)_2$ and 0.6 M $Fe(ClO_4)_3$ (upper right), yellow pale precipitates are observed. We note that similar precipitates are observed in DMF solution (bottom left) containing 0.7 M $Fe(ClO_4)_3$ without $Fe(ClO_4)_2$. On the other hand, no precipitates are observed in DMF solution (bottom right) without $Fe(ClO_4)_3$. This is because the solubility of $Fe(ClO_4)_2$ in DMF exceeded 2.0 M at 25 °C.

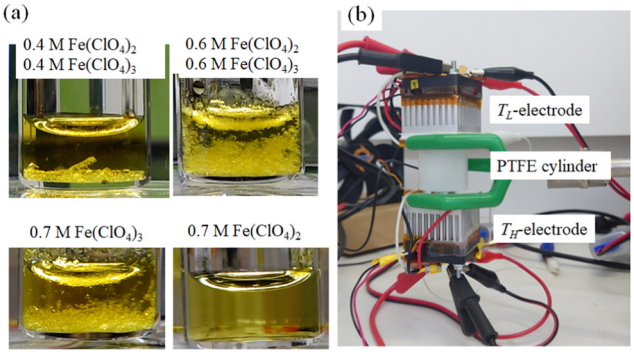

Fig. 2 (a) Photographs of DMF solution at 25 °C containing 0.4 M $Fe(ClO_4)_2$ and 0.4 M $Fe(ClO_4)_3$ (upper left), 0.6 M $Fe(ClO_4)_2$ and 0.6 M $Fe(ClO_4)_3$ (upper right), 0.7 M $Fe(ClO_4)_3$ (bottom left), and 0.7 M $Fe(ClO_4)_2$ (bottom right). The solution was heated to ~80 °C to melt the solute, then slowly cooled to 25 °C and left for a while. (b) Photograph of the thermocell.

We collected precipitates from DMF solution containing 0.5 M $Fe(ClO_4)_3$ and 0.5 M $Fe(ClO_4)_2$. The element ratio of N and C was evaluated by CNH elementary analysis using an organic elemental analyzer (UNICUBE, elementar). The ratio (N : C = 1.0 : 2.7) is close to the ratio of DMF (C_3H_7NO), indicating that the precipitate contains DMF molecules. We further evaluated the element ratio of Fe, Cl, O, and N with use of scanning electron microscopy (SEM-EDA: JSM-IT200; JOEL) equipped with an energy-dispersive X-ray analyzer. Table 1 shows the observed element ratio together with the calculated values with assuming $Fe(ClO_4)_x(C_3H_7NO)_y$. The optimized composition was $Fe(ClO_4)_{2.9}(C_3H_7NO)_{9.2}$. The composition indicates that the precipitate contains Fe^{3+}, but hardly any Fe^{2+}.

To quantitatively consider the precipitation effect of Fe^{3+}, the solubility s of Fe^{3+} in DMF solution was investigated. It is important to determine s in the same solution composition as

Table 1 Element ratio of precipitate in DMF solution containing 0.5 M $Fe(ClO_4)_3$ and 0.5 M $Fe(ClO_4)_2$. The element ratio was evaluated by SEM-EDA. The standard deviation was evaluated from six data points. In the calculation, the composition of the precipitate was assumed to be $Fe(ClO_4)_x(C_3H_7NO)_y$. The optimized composition is $Fe(ClO_4)_{2.9}(C_3H_7NO)_{9.2}$

	Fe	Cl	O	N
Observed	1	2.95(8)	20.89(2.84)	9.16(1.13)
Calculated	1	2.93	20.89	9.15

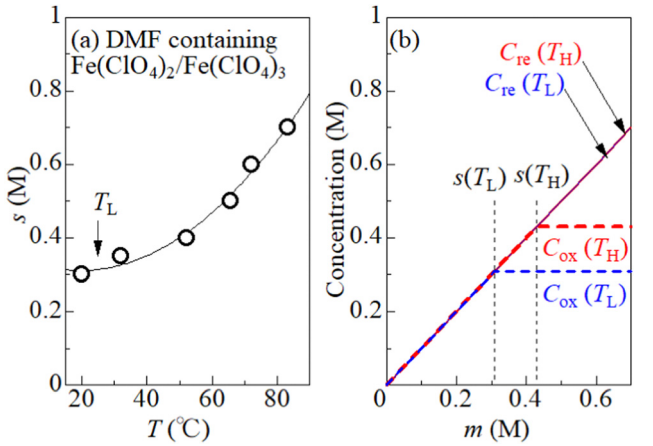

Fig. 3 (a) Solubility (s) of Fe^{3+} in DMF containing m M $Fe(ClO_4)_2$ and m M $Fe(ClO_4)_3$. T is the uniform temperature of the DMF solution. The solid curve is a result of least-squares fitting with a quadratic function. (b) Oxidant (C_{ox}) and reductant (C_{re}) concentrations against m at T_L = 25 °C and T_H = 55 °C.

for the measurement of V_T. This is because the dissolution of $Fe(ClO_4)_2$ can affect s through a change in $[ClO_4^-]$. We determine the maximum concentration (s) of equimolar $Fe(ClO_4)_2$ and $Fe(ClO_4)_3$ dissolved in DMF solution without precipitate containing Fe^{3+}. First, m^* M $Fe(ClO_4)_2$ and m^* M $Fe(ClO_4)_3$ were added to DMF. Then, the temperature of the solution was uniformly and slowly raised with stirring the solution. We carefully determined the temperature at which the solute completely melts. At that temperature (T), s becomes equal to m^*. We repeated the measurement for the respective m^*, and obtained a T–s data set. Open circles in Fig. 3(a) show the T–s data set. The solid curve is a result of least-squares fitting with a quadratic function.

Fig. 3(b) shows oxidant (C_{ox}) and reductant (C_{re}) concentrations against m at T_L = 25 °C and T_H = 55 °C. We note that s is the limit value of C_{ox}, that is, $C_{ox} = s$ if $s \leq m$. On the other hand, C_{re} (= m) is independent of s, because Fe^{2+} remains dissolved even if Fe^{3+} precipitates. Depending on the region of m, C_{ox} is expressed as $C_{ox}(T_L) = C_{ox}(T_H) = m$ for $m \leq s(T_L)$, $C_{ox}(T_L) = s(T_L)$ and $C_{ox}(T_H) = m$ for $s(T_L) \leq m \leq s(T_H)$, and $C_{ox}(T_L) = s(T_L)$ and $C_{ox}(T_H) = s(T_H)$ for $s(T_H) \leq m$.

2.2 Thermoelectromotive force

Thermoelectromotive force V_T was measured in a specially-designed thermocell[34] [Fig. 2(b)]. The electrolyte was filled in a 0.73 mm ϕ polytetrafluoroethylene (PTFE) cylinder. For the solution with $m \geq s(T_L)$ (= 0.32 M), the solution was heated to ~80 °C to dissolve the solutes before being sealed in the cell. Both ends were sealed with Al pedestals, on which the Pt disks were attached as the T_L- and T_H-electrodes. T_H and T_L were controlled with Peltier modules and monitored with T-type thermocouples. The electrode area and distance were 0.42 cm^2 and 1.0 cm, respectively.

V_T was measured against ΔT (= $T_H - T_L$) with fixing T_L at 25 °C. T_H was stepwisely controlled with the Peltier modules. V_T at each ΔT was measured under the open circuit condition with the use of a digital multimeter (Keithley 2100; Tektronics). α was evaluated by the slope of the $\Delta T - V_T$ plot.

2.3 Output characteristics of the LTE

The output characteristics of the LTE were investigated with the same thermocell as described in the previous subsection. In the measurement, ΔT, T_L, and T_H were fixed at 20 K, 25 °C, and 45 °C, respectively. The output voltage (V) was measured against current density (I). I was controlled by the external resistor (R_{ex}), which was connected in series with the LTE. The R_{ex} values were 10k, 3k, 1k, 240, 120, and 51 Ω. Considering the equivalent circuit, we obtained a relationship $V = IR_{ex} = V_T - IR_{in}$, where R_{in} is the internal resistance of the LTE. V at each R_{ex} was measured with the use of a digital multimeter (Keithley 2100; Tektronics). I at each R_{ex} was evaluated as $I = \frac{V}{R_{ex}}$.

3 Results

3.1 Precipitation enhancement of α

Fig. 4 shows ΔT–V_T plots against m. In the low m region below $s(T_L)$ (= 0.32 M), *i.e.*, at (a) 0.1 M and (b) 0.3 M, V_T increases in proportion to ΔT. The slope of the ΔT–V_T plot corresponds to α. The slope decreases with m from 1.43 mV K^{-1} at 0.1 M to

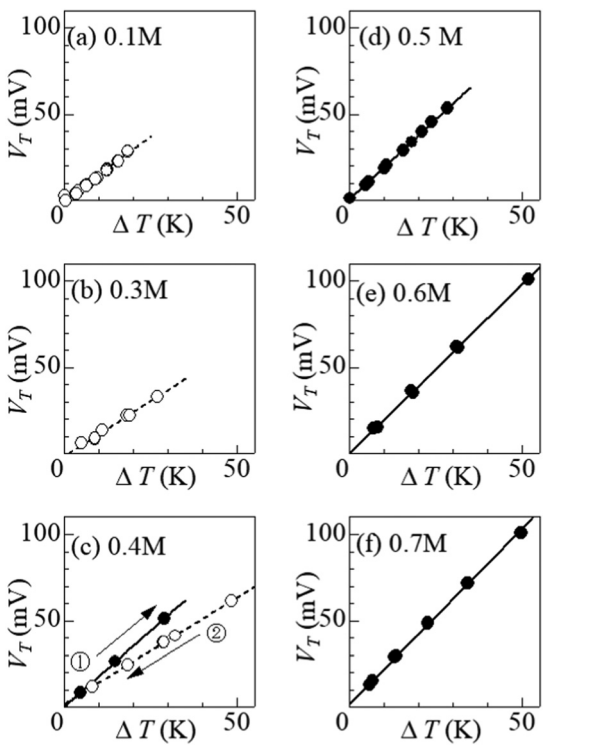

Fig. 4 Thermoelectromotive force V_T against temperature difference ΔT in DMF containing m M $Fe(ClO_4)_2$ and m M $Fe(ClO_4)_3$: (a) m = 0.1 M, (b) 0.3 M, (c) 0.4 M, (d) 0.5 M, (e) 0.6 M, and (f) 0.7 M. Closed and open circles correspond to electrolytes with and without precipitates, respectively. Straight lines are the results of least-squares fitting. Numbers in (c) indicate the order of measurements.

1.25 m K K^{-1} at 0.3 M. This is probably due to the overlap of the surrounding DMF molecules around iron ions.[26] The overlap of the solvent molecules effectively reduces the number of molecules affected by the redox reaction of the central ion, thereby suppressing ΔS in the reduction process. When m exceeds $s(T_L)$, a precipitation effect appears. At (c) 0.4 M, (d) 0.5 M, (e) 0.6 M, and (f) 0.7 M, the slopes of the ΔT–V_T plots (closed circles) are much larger than that (= 1.25 mV K^{-1}) at 0.3 M; 1.58 mV K^{-1} at 0.4 M in the ΔT-increasing run, 1.85 mV K^{-1} at 0.5 M, 1.96 mV K^{-1} at 0.6 M, and 2.04 mV K^{-1} at 0.7 M. Thus, we observed significant enhancement of α due to the precipitate containing Fe^{3+}.

Curiously, at (c) 0.4 M, the enhancement of α was significantly suppressed in the ΔT-decreasing run (open circles). We observed similar suppression of the enhancement also at 0.35 M. To investigate the cause of this phenomenon, we disassembled the 0.4 M thermocell immediately after the ΔT-decreasing run and examined the presence or absence of precipitates. We found no precipitates in the cell immediately after the ΔT-decreasing run. In the ΔT-increasing run, all the precipitates in the solution are considered to be dissolved at sufficiently large ΔT if $m \approx s$. The disappearance of precipitates at smaller ΔT in the ΔT-decreasing run is probably due to the supercooling effect. The supercooled state was found to be stable and was maintained for a long time in the measurement cell. At 0.4 M, the state was maintained for more than 20 hours at ΔT = 20 K, and for more than 10 hours at 10 K.

Fig. 5 shows α against m, which was evaluated by the slope of the ΔT–V_T plot. Closed and open circles correspond to with and without precipitates, respectively. The thin solid line is the result of least-squares fitting of the data below $m \leq 0.3$ M. We note that α (closed circles) with precipitation is much larger than the thin line. In the range of $0.35 \leq m \leq 0.40$, α (open circles) without precipitation is close to the thin line.

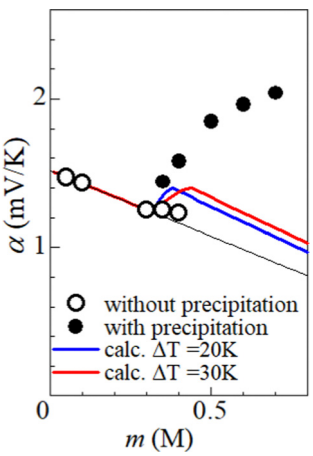

Fig. 5 Electrochemical Seebeck coefficient (α) against solute concentration m. Closed and open circles correspond to the observed data with and without precipitates, respectively. The thin straight line is the result of least-squares fitting of the data below 0.3 M without precipitation. The thick blue (red) curve is the calculation based on the concentration gradient model at ΔT = 20 K (30 K).

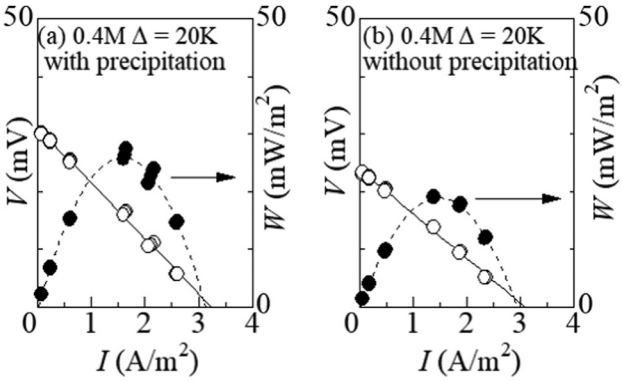

Fig. 6 Output voltage V and power density W against current density I in the LTEs at ΔT = 20 K at 0.4 M: (a) with and (b) without precipitation. Solid straight lines are the results of least-squares fitting. Broken curves are the result of least-squares fitting with a quadratic function.

3.2 Output characteristics of the LTE

Fig. 6 shows the I–V curve of the LTEs at ΔT = 20 K (a) with and (b) without precipitation. The latter performance was investigated in the LTE whose electrolyte was supercooled from $\Delta T \sim$ 50 K. In the (a) LTE with precipitates, the thermoelectromotive force and maximum power were 31.0 mV and 23.8 mW m^{-2}, respectively. In the (b) LTE without precipitation, the thermoelectromotive force and maximum power were 23.9 mV and 18.9 mW m^{-2}, respectively. The precipitates enhance V_T and the maximum power by as much as 30% and 32%, respectively.

4 Discussion

4.1 Concentration gradient effect

Now, let us discuss the origin of the enhanced α. The most probable origin for the enhancement is the concentration gradient effect.[30] Let us quantitatively evaluate the enhancement based on the Nernst equation (eqn (1)) including $s(T)$. By replacing the differential by dT with the difference by ΔT, α $\left(\equiv \frac{V(T_H) - V(T_L)}{\Delta T}\right)$ is expressed as

$$\alpha = \alpha_0 + \frac{k_B T_H}{\Delta T} \ln \frac{C_{ox}(T_H)}{C_{ox}(T_L)} + k_B \ln \frac{C_{ox}(T_L)}{m} \qquad (2)$$

where $\alpha_0 = \frac{\Delta V_0}{\Delta T}$. We note that $C_{re}(T_L) = C_{re}(T_H) = m$ in the present DMF solution containing m M $Fe(ClO_4)_2$ and m M $Fe(ClO_4)_3$. The first term α_0 corresponds to the normal component, which does not incorporate the effect of precipitation. Experimentally, the thin line in Fig. 5 corresponds to α_0. In the present system, α_0 is independent of T in the temperature range investigated. The second and third terms represent the concentration gradient effect and can be calculated using the experimentally obtained $s(T)$ of Fe^{3+}. We note that the second term is larger than the third one by a factor of $\frac{T_H}{\Delta T}$.

Let us investigate in detail the effect of T_H on the calculated α based on eqn (2). T_L was fixed at 25 °C in the present

experiment. Let us consider an electrolyte with precipitates at the T_L-electrode, *i.e.*, $s(T_L) \leq m$, and gradually increase T_H from T_L. If T_H is low enough so that $s(T_H) \leq m$ is satisfied, precipitates exist at both the T_L- and T_H-electrodes. In this temperature range, α depends on T_H *via* $C_{ox}(T_H)$ [$= s(T_H)$] and $\frac{T_H}{\Delta T}$ in the second term of eqn (2). With use of the least-squares fitted quadratic curve as $s(T)$ [Fig. 3(b)], we found that α gradually increases with T_H. If T_H becomes high enough so that $s(T_H) \geq m$ is satisfied, the precipitates melt at the T_H -electrodes, *i.e.*, $C_{ox}(T_H) = m$. In this temperature range, α monotonously decreases with T_H *via* $\frac{T_H}{\Delta T}$. Looking at Fig. 4, it is reasonable to compare the observed α with the calculated values at ΔT = 20–30 K.

We calculated α against m at ΔT = 20 and 30 K and plotted it by thick blue and red curves in Fig. 5, respectively. In the calculation, we used the least-squares fitted quadratic curve as $s(T)$, as indicated by the solid curve in Fig. 3(b). The enhancement of α is absent below $m \leq s(T_L)$ (= 0.32 M), because $C_{ox}(T_L) = C_{ox}(T_H) = m$. At ΔT = 20 K, the enhancement of α is almost constant above $m \geq s(T_H)$ (= 0.37 M), because $C_{ox}(T_L)$ [$= s(T_L)$] and $C_{ox}(T_H)$ [$= s(T_H)$] are independent of m. Similarly, the enhancement of α is almost constant above $m \geq s(T_H)$ (= 0.43 M) at ΔT = 30 K. In the region of $m \geq s(T_H)$, the enhancement of α is larger at ΔT = 30 K than that at 20 K. The calculation, however, cannot reproduce the observed α. Firstly, the calculated value is much smaller than the observed value. Secondly, the calculated value becomes constant above $m \geq 0.4$, while the observed value monotonously increases with m. To explain the observed α, additional precipitation effects are needed.

4.2 Solution-solid equilibrium of Fe^{3+}

The candidate for the additional precipitation effect is the chemical equilibrium effect of Fe^{3+} between the solution and solid (precipitate) phases [Fig. 1(b)]. Thermodynamically, α is equivalent to the entropy change ΔS during the reduction process divided by the elementary charge e. In the present Fe^{2+}/Fe^{3+} system, α without precipitation is positive. Then, the solution-solid equilibrium of Fe^{3+} further increases α as follows. The reduction reaction ($Fe^{3+} + e^- \rightarrow Fe^{2+}$) decreases the number of Fe^{3+} in solution. To compensate the decrease, Fe^{3+} in the nearby precipitate should dissolve into solution. The resultant solvation entropy of Fe^{3+} enlarges ΔS, and hence, α. For this process to occur, there must be active precipitates near the electrode surface where the reduction reaction takes place. Then, the enhancement of α is expected to increase with m, since the number of precipitates increases with m.

Now, let us evaluate the solvation entropy ΔS_{sol} in the solvation process of Fe^{3+} using a thermodynamic relation: $T\Delta S_{sol} = \Delta H - \Delta G$, where ΔH and ΔG are the enthalpy and Gibbs's free energy changes, respectively. ΔG is expressed as $\Delta G = -k_B T \ln Z_{sol}$, where Z_{sol} ($\equiv [Fe^{3+}][ClO_4^-]^3$) is the solubility equilibrium constant. We note that ΔG in this system is strongly temperature dependent around the LTE operating temperature, because Z_{sol}, or s [Fig. 3(b)], changes rapidly with T. With considering ΔS_{sol} and ΔH as constants, T-differential of $T\Delta S_{sol} = \Delta H - \Delta G$ gives $\Delta S_{sol} = -\frac{d\Delta G}{dT}$. By approximating the T-differential as the difference between 298 K (s = 0.32 M) and 328 K (s = 0.43 M), ΔS_{sol} was estimated to be 1.1 meV K^{-1}. The ΔS_{sol} value can fill the differences between the concentration gradient model at ΔT = 30 K and observed α, which ranges from 0.1 meV K^{-1} at 0.35 M to 0.9 meV K^{-1} at 0.7 M.

5 Conclusions

In conclusion, we systematically investigated α in DMF containing m M $Fe(ClO_4)_2$ and m M $Fe(ClO_4)_3$ against m. Above 0.35 M, we observed significant enhancement of α by precipitates containing Fe^{3+} and interpreted the enhancement in terms of the concentration gradient and solution-solid equilibrium effects. We further found that the precipitation enhances the LTE power at 0.4 M by as much as 32%.

Author contributions

Akihiko Waki: data curation; formal analysis; investigation. Dai Inoue: investigation (supporting). Yutaka Moritomo: conceptualization; supervision; and writing – original draft; writing – review & editing.

Conflicts of interest

There are no conflicts to declare.

Acknowledgements

This work was supported by the Yazaki Memorial Foundation for Science and Technology.

Notes and references

1 H. Wu, X.-L. Shi, J. Daun, Q. Liu and Z.-G. Chen, *Energy Environ. Sci.*, 2023, **16**, 1870.
2 H. Wu, X.-I. Shi, Y. Mao, M. L.i, W.-D. Liu, D.-Z. Wang, L.-C. Yin, M. Zhu, Y. Wang, J. Duan, Q. Liu and Z.-G. Chen, *Adv. Energy Matter.*, 2023, **13**, 2302551.
3 X.-L. Shi, H. Wu, Q. Liu, W. Zhou, S. Lu, Z. Shao, M. Dargusch and Z.-G. Chen, *Nano Energy*, 2020, **78**, 105195.
4 A. Schiraldi, E. Pezzati and P. Baldini, *J. Phys. Chem.*, 1985, **89**, 1528.
5 T. Ikeshoji, *Bull. Chem. Soc. Jpn.*, 1987, **60**, 1505.
6 I. Quickenden and Y. Mua, *J. Electrochem. Soc.*, 1995, **142**, 3985.
7 Y. Mua and T. I. Quickenden, *J. Electrochem. Soc.*, 1996, **143**, 2558.
8 R. Hu, B. A. Cola, N. Haram, J. N. Barisci, S. Lee, S. Stoughton, G. Wallace, C. Too, M. Thomas, A. Gestos, M. Ed Cruz, J. P. Ferraris, A. A. Zakhidov and R. H. Baughman, *Nano Lett.*, 2010, **10**, 838.

9 D. R. MacFarlane, N. Tachikawa, M. Forsyth, J. M. Pringle, P. C. Howlett, G. D. Elliott, J. F. Davis, Jr., M. Watanabe, P. Simon and C. A. Angell, *Energy Environ. Sci.*, 2014, **7**, 232.
10 M. Bonetti, S. Nakamae, M. Roger and P. Guenoun, *J. Chem. Phys.*, 2011, **134**, 114513.
11 T. J. Abraham, D. R. MacFarlane and J. M. Pringle, *Chem. Commun.*, 2011, **47**, 6260.
12 M. Romano, S. Gambhir, J. Razal, A. Gestos, G. Wallace and J. Chen, *J. Therm. Anal. Calorim.*, 2012, **109**, 1229.
13 M. S. Romano, N. Li, D. Antiohos, J. M. Razal, A. Nattestad, S. Beirne, S. Fang, Y. Chen, R. Jalili, G. G. Wallace, R. Baughman and J. Chen, *Adv. Mater.*, 2013, **25**, 6602.
14 T. J. Abraham, D. R. MacFarlane and J. M. Pringle, *Energy Environ. Sci.*, 2013, **6**, 2639.
15 A. Gunawan, C.-H. Lin, D. A. Buttry, V. Mujica, R. A. Taylor, R. S. Prasher and P. E. Phelan, *Nanoscale Microscale Thermophys. Eng.*, 2013, **17**, 304.
16 N. Jiao, T. J. Abraham, D. R. MacFarlane and J. M. Pringle, *J. Electrochem. Soc.*, 2014, **161**, D3061.
17 S. Uhl, E. Laux, T. Journot, L. Jeandupeux, J. Charmet and H. Keppner, *J. Electron. Mater.*, 2014, **43**, 3758.
18 A. Gunawan, H. Li, C.-H. Lin, D. A. Buttry, V. Mujica, R. A. Taylor, R. S. Prasher and P. E. Phelan, *Int. J. Heat Mass Trans.*, 2014, **78**, 423.
19 M. A. Lazar, D. Al-Masri, D. R. MacFarlane and J. M. Pringle, *Phys. Chem. Chem. Phys.*, 2016, **18**, 1404.
20 H. Im, T. Kim, H. Song, J. Choi, J. S. Park, R. Ovalle-Robles, H. D. Yang, K. D. Kihm, R. H. Baughman, H. H. Lee, T. J. Kang and Y. H. Kim, *Nat. Commun.*, 2016, **7**, 10600.
21 A. H. Kazim and B. A. Cola, *J. Electrochem. Soc.*, 2016, **163**, F867.
22 M. Sindhuja, B. Lohith, V. Sudha, G. R. Manjunath and S. Harinipriya, *Mater. Res. Express*, 2017, **4**, 075513.
23 J. H. Kim, J. H. Lee, E. E. Palen, M.-S. Suh, H. H. Lee and R. J. Kang, *Sci. Rep.*, 2019, **9**, 8706.
24 M. A. Buckingham, F. Marken and L. Aldous, *Sustainable Energy Fuels*, 2018, **2**, 20717.
25 A. Wake, D. Inoue and Y. Moritomo, *Appl. Phys. Express*, 2022, **15**, 054002.
26 A. Wake, D. Inoue and Y. Moritomo, *Jpn. J. Appl. Phys.*, 2023, **62**, 014002.
27 H. Zhou, T. Yamada and N. Kimizuka, *J. Am. Chem. Soc.*, 2016, **138**, 10502.
28 Y. Liang, J. K.-H. Hui, M. Morikawa, H. Inoue, T. Yamada and N. Kimizuka, *Appl. Energy Matter.*, 2021, **4**, 5326.
29 J. Duan, G. Feng, B. Yu, J. Li, M. Chen, P. Yang, J. Feng, K. Liu and J. Zhou, *Nat. Commun.*, 2018, **9**, 5146.
30 B. Yu, J. Duan, H. Cong, W. Xie, R. Liu, X. Ahuang, H. Wang, B. Qi, M. Xu and L. Wan, *Science*, 2020, **370**, 342.
31 T. Kim, J. S. Lee, G. Lee, H. Yoon, J. Yoon, T. J. Kangd and Y. H. Kim, *Nano Energy*, 2017, **31**, 160.
32 Y. Xaing, X. Guo, H. Zhu, Q. Zhang and S. Zhu, *Chem. Eng. J.*, 2019, **461**, 142013.
33 D. Inoue, H. Niwa, H. Nitani and Y. Moritomo, *J. Phys. Soc. Jpn.*, 2021, **90**, 033602.
34 Y. Fukuzumi, Y. Hinuma and Y. Moritomo, *Jpn. J. Appl. Phys.*, 2019, **58**, 065501.